Journal of *Marine Science and Engineering*

MDPI

Article

Radiation Hazard from Natural Radioactivity in the Marine Sediment of Jeddah Coast, Red Sea, Saudi Arabia

Bandar A. Al-Mur [1] and Ahmed Gad [2,*]

[1] Environmental Science Department, Faculty of Meteorology, Environment and Arid Land Agriculture, King Abdulaziz University (KAU), Jeddah 21589, Saudi Arabia
[2] Geology Department, Faculty of Science, Ain Shams University, Cairo 11566, Egypt
* Correspondence: a.gad@sci.asu.edu.eg

Abstract: Marine sediment samples were collected along the Jeddah coast, Red Sea, Saudi Arabia, in order to assess radiation hazards and the exposure to human and marine living organisms. Using collaborative techniques, grain size, mineralogical characteristics, and natural radioactivity were investigated. To examine the influence of sediment characteristics over the distribution of the measured radionuclides, resulting data were statistically processed by using multivariate analyses. ^{238}U, ^{232}Th, and ^{40}K levels were specified to be 19.50, 9.38, and 403.31 Bq kg^{-1}, respectively. Radionuclides distributions were affected by sediment mud content, organic matter, and heavy minerals index. The calculated radiation risk parameters are within the safe range and lower than the global average. Natural radiation from these marine sediments is normal and poses no significant radiological risk to the public or marine living organisms. The natural radioactivity of the marine sediment in this Jeddah coastline will have to be monitored on a regular basis to avoid overexposure to the residents.

Keywords: marine sediment; radionuclides; radiation hazards; non-human biota; mineralogy; Red Sea; Jeddah

Citation: Al-Mur, B.A.; Gad, A. Radiation Hazard from Natural Radioactivity in the Marine Sediment of Jeddah Coast, Red Sea, Saudi Arabia. *J. Mar. Sci. Eng.* **2022**, *10*, 1145. https://doi.org/10.3390/jmse10081145

Academic Editors: Anabela Tavares Campo Oliveira and Intae Kim

Received: 4 July 2022
Accepted: 16 August 2022
Published: 19 August 2022

1. Introduction

Scientists, international organizations, and laypeople are increasingly agreeing that human exposure to ionizing radiation represents a terrible and unavoidable environmental issue. Public exposure to radiation come from naturally occurring (primordial) and artificial (fall-out) radionuclides, with the majority from natural sources [1–3]. Naturally occurring radionuclides such as Uranium-238 (^{238}U), Thorium-232 (^{232}Th), and Potassium-40 (^{40}K) are abundant in the Earth's continental crust [4,5]. These radionuclides can be found in different environmental components, including rocks, soil, stream sediment, groundwater, surface water, marine sediment and water, and biota [6–11].

The coastal ecosystem supports a diverse range of inorganic and bio-resources, many of which, in common fishery, are commercially, culturally, scientific, aesthetically, and recreationally important to the people of the entire region. The study of various bio-resources and associated geological processes of the coastal zone improves the proper understanding of the relationship between biotic and non-biotic components and their mutual dependence on maintaining ecosystem integrity [12,13]. Marine sediments play an important role in the ecology and environment of coastal ecosystems and marine environments. They are constantly changing and are the most dynamic part of these ecosystems [14,15]. Numerous marine contaminants, including radionuclides, are stored in marine sediments. Anthropogenic activities have contributed to the radioactivity level in marine ecosystems. Industrial discharges, nuclear accidents, and the discharge of nuclear waste have been recognized as main sources of elevated radioactivity levels in many marine ecosystems [16–18]. Lin et al. [19] recorded anthropogenic uranium imprints in the Baltic Sea sediments due to human nuclear-related activities. Al-Qasmi et al. [20] ascribed the enrichment of ^{238}U, ^{236}U, and ^{234}U in the marine sediment from Loch Etive, Scotland, to the

uranium released from the phosphate plant and Sellafield nuclear-fuel reprocessing facility. Pappa et al. [21] reported enhanced values of ^{226}Ra and ^{235}U in Stratoni port, Greece, due to mining-related activities. Aközcan et al. [22] recorded an extraordinary increase in the background levels of ^{226}Ra and ^{40}K in Bafa Lake, Turkey; these hot spots were attributed to industrial and agricultural activities. Diab et al. [23] noticed a slight increase in ^{238}U and ^{232}Th levels due to oil exploration and production activities in Egypt's Gulf of Suez. Influences of the Chernobyl disaster are still noted in the marine sediments of numerous European countries such as the Gulf of Bothnia [24], Swedish coast [25], Amvrakikos Gulf (Greece) [26], Vefsnfjord (Norway) [27], Black Sea [28], and Baltic Sea [19]. Radionuclides released from the Fukushima accident have been transported long distances within the Pacific Ocean and are stored in marine sediments [29,30].

These radionuclides can accumulate in marine biota via sediment and water and demonstrate biomagnifications through trophic levels. Consequently, these radioactive elements enter the food chain through the direct consumption of marine foods [4,7,13,31,32]. Radionuclides in marine sediments are frequently used as radiotracers to better understand sedimentological, morphodynamics, and oceanographic processes and to reconstruct pollution events in the past [18,33]. The detection of radionuclides in sediments contributes significantly to human background radiation exposure and provides vital information on human and ecosystem health effects of natural radioactivity [4,23,34]. In addition, it can provide a critical foundation for evaluating any inadvertent release of radioelements for the better management and conservation of marine resources [18].

Lately, considerable emphasis has been dedicated to the development of a scientific database of radiation baselines in the Middle East, particularly in Arab nations, considering their ambitious intentions to construct nuclear and renewable energy capacities. For example, the United Arab Emirates launched the Arabian Gulf region's first nuclear program by constructing four nuclear reactors [35,36]. Egypt has begun restarting its ambitious program to construct nuclear power reactors [37]. Saudi Arabia's nuclear energy ambitions are in the initial stages, and the country recently revealed a proposal for nuclear power development that will be completed by 2040 [36,38,39]. The construction of a nuclear research reactor in Saudi Arabia is almost finished. Saudi Arabia's Red Sea coastline contains many promising sites for nuclear power plant construction [36,40]. The baseline data could be used to analyze any changes in the radiation background level caused by radioactive substances-related activities.

The Red Sea is a complicated marine ecosystem that has unique biodiversity, as well as a vital maritime lane that connects the world's major oceans for global trade and commerce [41,42]. Saudi Arabia has rapidly progressed from a developing state with serious limitations to an ambitious industrialized country. Saudi Arabia's Red Sea coastline is densely populated and is thought to be more conducive to many different types of sustainable economic-development and blue economy activities [41]. Influences of large-scale human activities on the Red Sea's environmental compartments have heightened in recent years, and these influences are now of significant concern [41,43–45]. There is a scarcity of data on the radioactivity level in Saudi Arabia's coastal regions along the Red Sea [41]. Environmental radioactivity studies were concentrated in the Arabian Gulf [46–49]. The study area chosen for this study represents a result of recent industry developments in the Jeddah coastline over the last two decades. There are no available data about the natural radioactivity levels in Jeddah area. Thus, the present study attempt to (1) determine the levels of natural radioactivity in Jeddah coastline marine sediments, (2) compare the obtained results with literature, and (3) investigate the radiation hazard for members of the public and marine non-human biota due to exposure to natural radiation. This study will contribute to the radiation data bank of Saudi Arabia.

2. Materials and Methods

2.1. The Study Area

The study area covers the coastal of Jeddah, Red Sea, Saudi Arabia, between latitudes 20°56′50″ and 21°11′30″ N and longitudes 39°8′40″ and 39°19′40″ E (Figure 1). Jeddah city is considered one of the most significant and largest (1765 km^2) urban and industrial areas along Saudi Arabia's Red Sea coastline. It is characterized by an arid climate with sparse rainfall [43,50].

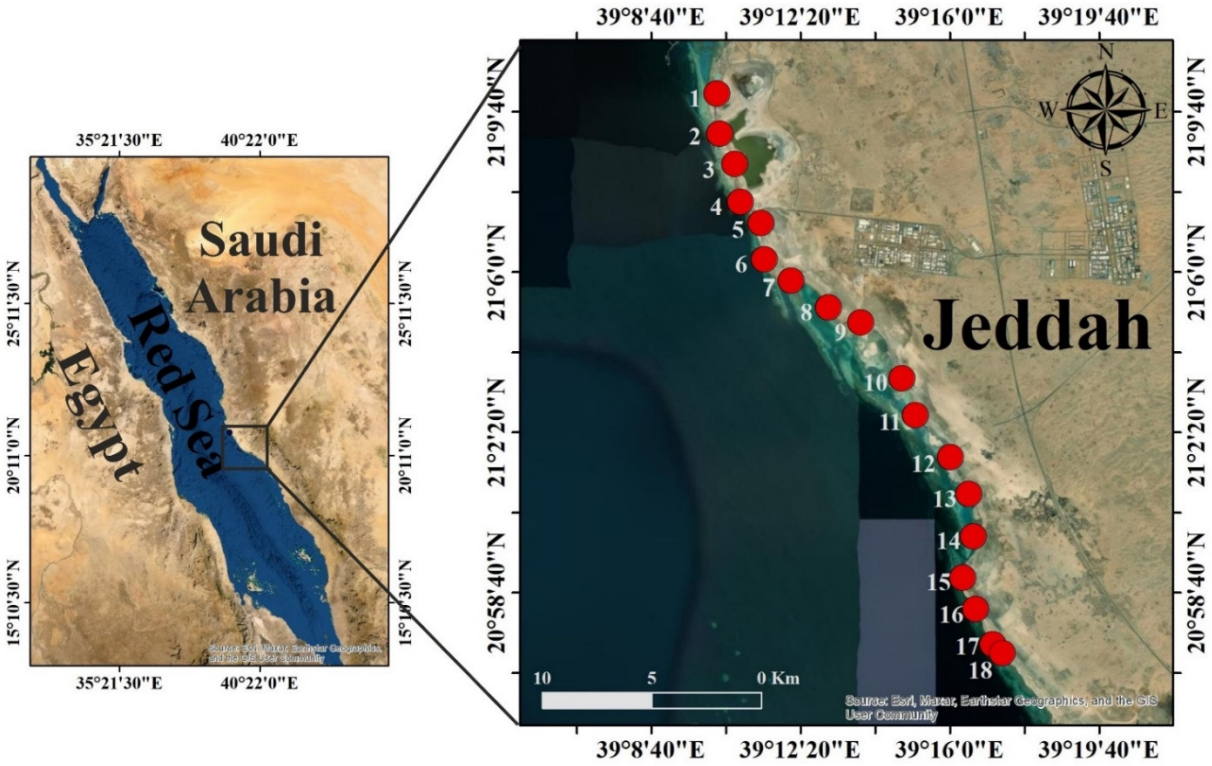

Figure 1. The study area and sampling site's locations.

Jeddah is part of the eastern Red Sea shelf region, bordered on land by the rough Arabian Shield mountains. These mountains represent Neoproterozoic basement rocks, which include Precambrian calc-alkaline volcanic, volcaniclastic, intrusive, and metamorphic rocks. Tertiary clastic succession, basaltic lavas, and gabbro dikes cover these basement rocks. Quaternary surficial deposits cover the coastal plain, including coral reefs and carbonate, alluvial deposits, sabkha, and sand dunes [15,51].

The Red Sea is unique among the world's seas in that it has a few permanent streams flowing into it and receives extremely scanty irregular rainfall. Terrigenous sediments are contributed by mostly northwesterly winds and occasional rainstorms. Aeolian and biogenic materials contribute significantly to the marine realm in arid regions such as Saudi Arabia, where riverine sediments are rare or completely absent [50,52].

2.2. Sampling and Sample Treatment

Eighteen sampling sites representing the surface marine sediments (0–10 cm depth) were selected for this study (Figure 1). Approximately 500 g of sediment samples was collected during March 2020 using a Van-Veen grab sampler by combining three subsamples from each site. In order to prevent cross-contamination, the collected samples were transferred to new, clean, and labelled plastic jars using a clean stainless-steel shovel. The samples were immediately stored in ice boxes under −4 °C until transportation to the lab. The sediment samples were blended, homogenized, and dried at room temperature before being placed in an electric oven (105 °C; 24 h) to dispose of the moisture and to achieve

a constant weight [9,28,32]. These samples were then divided into several portions for various laboratory examinations.

2.3. Sediment Granulometry and Mineralogy

Utilizing loss in ignition methods [53], organic matter content (OM%) was determined in the sediment. Following digestion in HCl (1 N), the gravimetric technique was used to calculate $CaCO_3$ concentrations [54]. Wet sieving was used to calculate the proportions of the different particle size grades (sand 2.00–0.063 mm and mud < 0.063 mm) [55]. Heavy minerals were separated using heavy liquid technique (Bromoform) and examined using a polarizing microscope [56,57]. The mineralogical compositions of the bulk powdered sediment samples were determined by using the X-ray diffraction technique (XRD). The qualitative chemical composition of selected heavy mineral grains were examined utilizing environmental scanning electron microscope (ESEM) and energy dispersive spectrometer (EDS) techniques (SEM/EDX, XL 30 ESEM, Philips Co., Amsterdam, The Netherlands). Extensive technical descriptions of OM% and $CaCO_3$%, grain size and heavy minerals determination and the specification of SEX/EDX and XRD instruments are provided in Table S1 (in Supplementary Materials).

2.4. Radiometric Analysis

Dried and homogenized marine sediment samples were weighed and instantly placed into a 100 mL plastic standard cylinder and firmly sealed using Teflon tape around their screw necks, and wide Vinyl tape was used around their caps and secured for 30 days until examination. The radiogenic gases ^{222}Rn and ^{220}Rn are prevented from escaping by the in-growth of U and Th decay, which additionally allows for secular equilibrium between ^{238}U, ^{232}Th, and their decay products [58]. A well-calibrated sodium-iodide and thallium-activated gamma-ray spectrometry scintillation detector (3″ × 3″ NaI (Tl)) was used to specify the amounts of ^{238}U (^{234}Th-0.0633 MeV), ^{232}Th (^{212}Pb-0.2386 MeV) and ^{40}K (1.461 MeV) activity concentrations in the collected marine sediment samples. This detector is sealed with a photomultiplier tube in aluminum housing. The tube is adequately protected against induced X-rays by a cylindrical copper (0.6 cm thickness) and isolated from environmental radiation by a chamber of lead bricks and lead cover (5 cm). Standard point sources (^{60}Co and ^{137}Cs) were used to calibrate the detector's energy. Every sample has been counted for 1000 s. Additional details for the exact calculation of the activity concentration can be obtained from the literature [4,5].

Samples preparation, grain size analysis and heavy minerals separation were conducted at the Geology Department, Faculty of Science, Ain Shams University Laboratories. The XRD analysis were carried out at the Central Laboratories Sector of The Egyptian Mineral Resources Authority. SEM/EDX and radiometric analysis were performed at the Egyptian Nuclear Materials Authority.

2.5. Calculation of the Radiation Hazard Indices

The radium equivalent activity index (Ra_{eq}) [1,59], external hazard index (H_{ex}) [1,60], absorbed dose rate (D) [1], annual effective dose (AEDE) [1], and excess lifetime cancer risk (ELCR) [6,61,62] have all been calculated in order to evaluate the external radiation hazards brought on by the activity concentration of the measured radionuclides in the marine sediment of the Jeddah Coast, Red Sea, Saudi Arabia. Table S2 (in Supplementary Materials) provides an overview of the descriptions and formulas used to calculate external hazard indicators.

The total dose rate (TD) per organism to biota (non-human) in the marine environments was calculated utilizing the ERICA Tool software (ERICA tool version 2.0.185, https://erica-tool.com/, accessed on 3 July 2022) [63]. The ERICA software is a dosimetry model that calculates the internal and external absorbed dose rates to (marine living organisms across a broad range of body masses and habitats for all radioactive elements of

concern (^{238}U and ^{232}Th). The ERICA tool is thoroughly described in the literature [63,64]; more details can be found in Table S1.

2.6. Statistical Analyses

To reveal and emphasize the interrelationship between the investigated radionuclide (^{238}U, ^{232}Th, and ^{40}K) activity concentrations and sediment properties (grain size, $CaCO_3$, OM, and Heavy Minerals index), a multivariate Pearson's correlation coefficient matrix (PCC), hierarchical cluster analysis (HCA) in Q mode, and principal component analysis (PCA) were performed using SPSS (version 21.0, New York, NY, USA) and OriginLab (version OriginPro 2021, Northampton, MA, USA).

3. Results and Discussion

3.1. Textural Attributes

Findings of grain-size analysis of the collected marine sediment samples are provided in Table 1. Their $CaCO_3$ contents varied from 6.80 to 62.80%, these sediments are generally rich in carbonate. The organic matter content (OM%) of these sediments ranged from 0.00 to 1.20%. The low OM observed in these sediments can be explained by the deposition of siliciclastic terrigenous materials, which are low in OM or by rapid degradation of recently formed, easily decomposable endogenic biological activity [65]. Compared to mud fraction (silt and clay), sand fractions were found to be dominant in all studied samples (23.00–92.80%). On the other hand, the mud fraction has no clear trend. It is obvious that these sediments are composed mainly of carbonate and sand with minor amounts of mud and OM. The carbonate content in these coastal sediments is sourced from the erosions of carbonate-rich coastal rocks and the mixing of sediments with shell fragments and other calcareous debris [44,66,67].

Table 1. Grain size data, heavy minerals index, and activity concentration of the measured radionuclides.

Sample No.	$CaCO_3$ %	OM %	Sand% (2.00–0.063 mm)	Mud% (<0.063 mm)	Heavy Minerals%	^{238}U (Bq kg^{-1})	^{232}Th (Bq kg^{-1})	^{40}K (Bq kg^{-1})
1	44.00	0.20	50.60	5.20	4.96	39.72	12.64	387.38
2	21.40	0.00	78.60	0.00	3.94	12.43	4.14	387.45
3	7.60	0.00	77.80	14.60	6.44	24.35	8.28	433.87
4	18.00	0.00	75.80	6.20	10.08	24.86	12.13	356.39
5	38.80	0.20	56.80	4.20	8.12	12.47	8.26	472.61
6	25.00	0.00	75.00	0.00	5.30	12.22	8.34	470.02
7	17.00	0.00	74.00	9.00	15.16	37.29	16.17	315.07
8	6.80	0.00	92.80	0.40	6.06	12.92	8.54	454.53
9	19.20	0.20	75.80	4.80	6.32	12.43	8.22	449.36
10	62.80	1.20	23.00	13.00	2.44	37.77	8.82	338.31
11	54.60	0.40	39.40	5.60	4.38	24.74	8.55	250.51
12	56.80	0.40	38.40	4.40	4.02	12.35	8.17	253.09
13	50.20	0.00	48.60	1.20	8.90	12.47	16.17	317.65
14	15.40	0.40	84.20	0.00	10.90	12.41	12.24	557.83
15	50.40	0.20	49.00	0.40	4.06	12.38	4.04	374.47
16	42.40	0.00	57.20	0.40	0.48	24.95	8.05	537.17
17	47.80	0.00	52.00	0.20	0.56	12.93	8.08	444.20
18	48.20	0.00	51.20	0.60	2.54	12.28	8.05	459.69
Min.	6.80	0.00	23.00	0.00	0.48	12.22	4.04	250.51
Max.	62.80	1.20	92.80	14.60	15.16	39.72	16.17	557.83
Mean	34.80	0.18	61.12	3.90	5.81	19.50	9.38	403.31

3.2. Mineralogy

The mineral composition of representative bulk sediment samples (Figure S1) revealed the dominance of silicate minerals (quartz, albite, and amphiboles) and non-silicate minerals (calcite, aragonite, and gypsum). The heavy minerals indices of the studied marine sediments range from 0.48% and 15.16% (mean 5.81%).

The light minerals fractions of these marine sediments consist mostly of quartz and feldspar grains (mainly albite). Both opaque and non-opaque minerals varieties identified within the heavy mineral assemblage. The opaque minerals are mostly magnetite, ilmenite, and chromite (Figure 2). The non-opaque minerals assemblages consist of amphiboles, pyroxenes, epidote, zircon, sphene, garnet, monazite, tourmaline, and kyanite (Figure 3). Andalusite, rutile, and staurolite were recorded in a few samples in minor amounts. Interestingly, monazite grains show U and Th concentrations in their chemical composition (Figure 4). Monazite is thought to be the primary source of natural radioactivity in marine and beach sand [68–72].

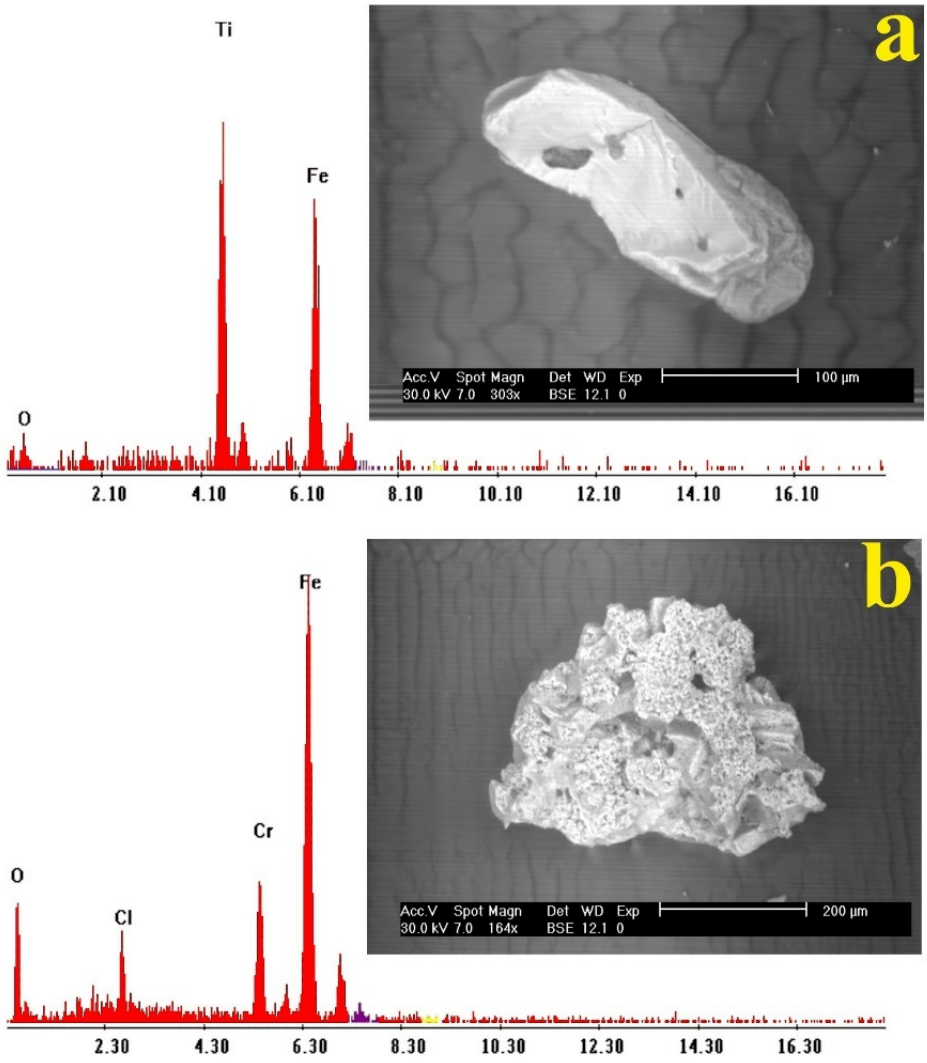

Figure 2. SEM/EDX of (**a**) ilmenite (sample 3) and (**b**) chromite (sample 3).

Figure 3. Photomicrographs of identified heavy minerals.

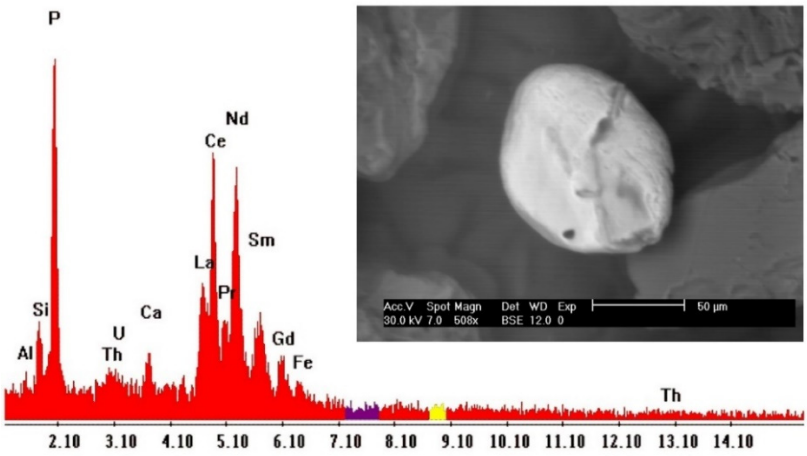

Figure 4. SEM/EDX of monazite (sample 1).

The heavy mineral assemblages of Jeddah coastal marine sediments are, to a large extent similar, suggesting inheritance from the same source rocks. The nature of these assemblages indicates a variety of probable source rocks, including sedimentary, igneous, and metamorphic, with a relatively short distance of transportation. This explains the distinctly low roundness of the heavy grains (Figure 3) and the considerable amounts of feldspars grains. The distinctly high proportions of amphiboles and pyroxenes in the marine sediments studied indicate a major role of the surrounding basement. The potential contribution of a metamorphic rock source has pointed to the presence of garnet, kyanite, staurolite, and andalusite [57,73]. These results are consistent with many research studies [52,66,74].

3.3. Activity Concentrations

Table 1 lists the measured activity concentrations of ^{238}U, ^{232}Th, and ^{40}K in the investigated marine sediment. These values are presented by graduated symbols method in Figure 5. The activity concentrations of the measured radionuclide have the order of ^{40}K > ^{238}U > ^{232}Th. The results clearly reveal that the observed concentration of ^{40}K greatly surpasses those of both ^{238}U and ^{232}Th. This indicates that ^{40}K in common is a more prevalent radioactive element in these marine sediments. Potassium is more abundant in magmatic rocks as a major constituent of several rock-forming minerals than U and Th [75–77]. The activity concentration of ^{238}U, ^{232}Th, and ^{40}K varied site-by-site, because the physical, chemical, geochemical, and mineralogical components of the marine sediment vary greatly [78,79]. The mean concentration values of ^{238}U, ^{232}Th, and ^{40}K are 19.50 Bq kg^{-1}, 9.38 Bq kg^{-1}, and 403.31 Bq kg^{-1}; respectively. These mean values are significantly lower than the world average [6] (Table 2). The current investigation revealed that ^{238}U, ^{232}Th, and ^{40}K levels in marine sediment of Jeddah coastline are remarkably natural.

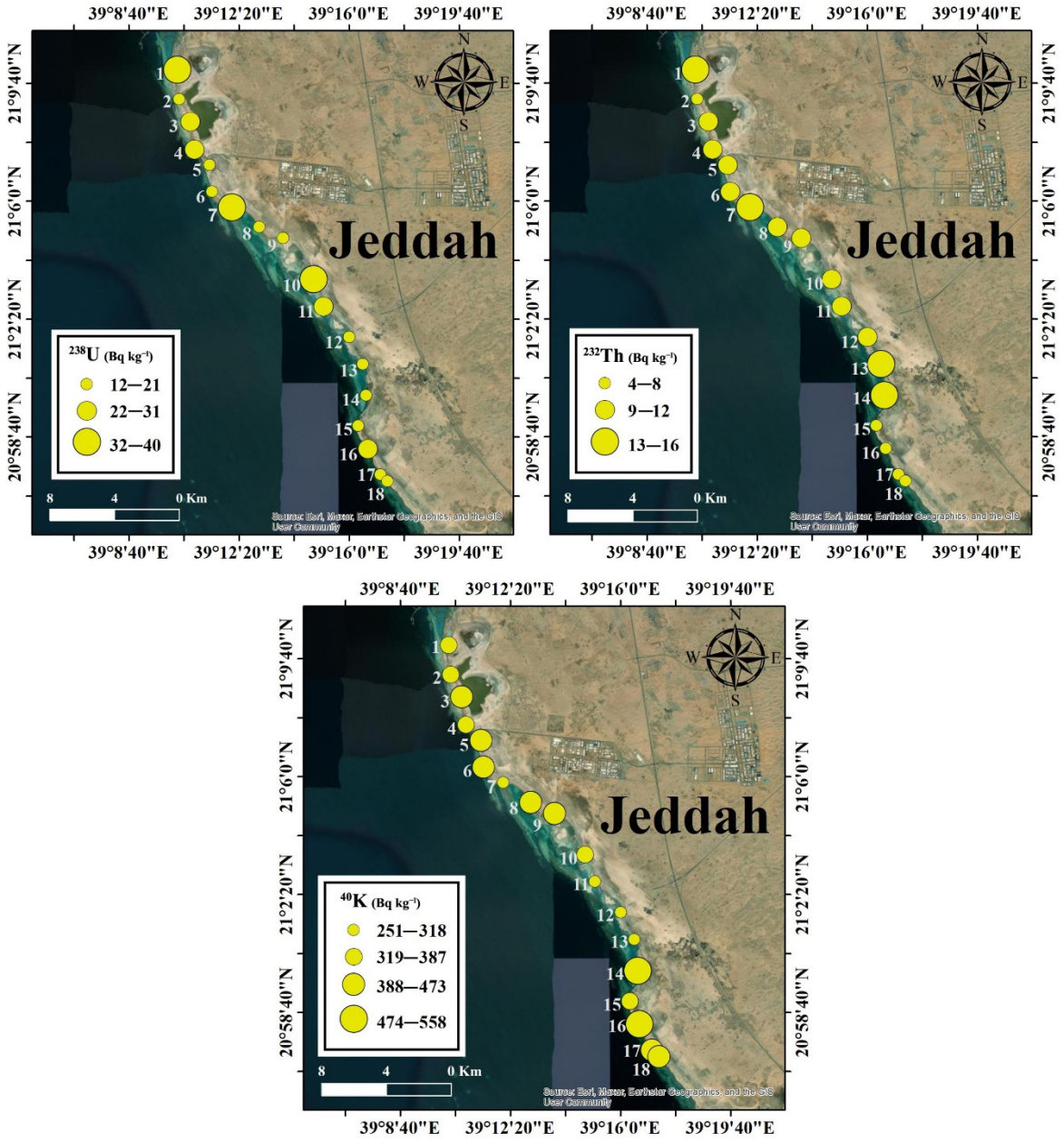

Figure 5. Distribution pattern maps of ^{238}U, ^{232}Th, and ^{40}K activity concentrations.

We attempted to compile a recent comparison of natural radiation levels in marine sediment from various regions of Saudi Arabia and those worldwide. Table 2 showed that the mean values of ^{238}U in the Jeddah marine sediment were lower than that reported in Saudi Arabia and other countries except for the Arabian Gulf [48], Addurrah beach [49], Egyptian Gulf of Suez [23], Egyptian Mediterranean Sea [69], and Turkey [80]. The mean activity concentrations of ^{232}Th in Jeddah marine sediments were lower than all other locations in the world except for the Arabian Gulf [48], Farasan Island [46], Oman [81], and Turkey [80]. Conversely, the ^{40}K mean values were higher than all other locations in the world except Addurrah beach [49], Serbia [82], Cyprus [4], and Bangladesh [32]. It is worth noting that U and Th series disequilibria were well documented [31,83]. The presented values of ^{226}Ra and ^{228}Ra (Table 2) do not assume that there are ^{238}U/^{226}Ra and ^{232}Th/^{228}Ra equilibria in those samples; they are merely displayed for simple comparisons.

Table 2. Comparison of ^{238}U, ^{232}Th, and ^{40}K mean activity concentration in marine sediment and sand samples reported for different region in Saudi Arabia and worldwide.

Location	Samples	^{238}U Series *	^{232}Th Series **	^{40}K	Reference
Saudi Arabia					
Jeddah	Marine Sediment (N = 18)	19.50	9.38	403.31	Present study
Arabian Gulf	Marine Sediment (N = 9)	3.50 *	5.90 **	113.50	[48]
Arabian Gulf	Marine Sediment (N = 12)	26.40 *	16.30	351.00	[47]
Arabian Gulf	Beach sand (N = 12)	22.70 *	14.80	392.00	[47]
Farasan Island	Marine Sediment (N = 8)	35.46	1.84	34.34	[46]
Gulf of Aqaba (Addurrah beach)	Marine Sediment (N = 19)	16.97	22.48	641.08	[49]
Worldwide					
World average		32	45	412	[6]
Egypt (Gulf of Suez)	Shore Sediment (N = 36)	13.79	14.55	128.67	[23]
Egypt (Red Sea)	Marine Sediment (N = 84)	23.80 *	19.60	374.90	[84]
Egypt (Mediterranean Sea)	Beach sand (N = 12)	8.80 *	30.80	106.9	[69]
Oman	Marine Sediment (N = 11)	20.49	2.26	44.83	[81]
Iran (Caspian Sea)	Marine Sediment (N = 8)	34.40 *	11.40	310.00	[9]
Serbia (Boka Kotorska Bay)	Marine Sediment (N = 12)	37.00	35.00	580.00	[82]
Cyprus (East coast region)	Marine Sediment (N = 15)	23.00 *	19.00	628.10	[4]
China (Beibu Gulf)	Marine Sediment (N = 50)	25.90	37.6	263	[85]
India (Tamilnadu)	Beach sand (N = 101)	47.04	26.63	372.49	[86]
Bangladesh (Bay of Bengal)	Offshore Sediment (N= 6)	31.20	51.90	686.40	[32]
Turkey (Kocaeli- black sea)	Beach sand (N = 20)	8.85	8.93	219.41	[80]
Ghana (Tema Harbour)	Marine Sediment (N = 21)	34.00	30.00	320.00	[31]
Nigeria (Akwa Ibom)	Beach Sediment (N = 15)	23.00	36.00	145.00	[2]

* ^{226}Ra activity concentration. ** ^{228}Ra activity concentration.

3.4. Multivariate Statistical Analyses

A comparative PCC (Table 3) analysis was conducted to pinpoint the direct association between the specific characteristics of the considered marine sediments and ^{238}U, ^{232}Th, and ^{40}K. Correlations of 0.20–0.39, 0.40- 0.59, 0.60–0.79, and 0.80–1.00 are considered weak, moderate, strong, and very strong, respectively [87]. ^{238}U has significant strong positive correlations with mud content (Pearson's R = 0.678) and weak positive correlation with OM (Pearson's R = 0.357), indicating the effect of fine particles and OM on the distribution of ^{238}U [37]. ^{238}U has moderate positive correlations with ^{232}Th (Pearson's R = 0.419), this is due to the co-existence of U and Th radionuclides in nature [69,85,88], which is reflected by the presence of both radioelements in the SEM/EDX of monazite grain (Figure 4). ^{232}Th has significant strong positive correlations with heavy minerals index (Pearson's R = 0.696). On the other hand, ^{40}K has moderate positive correlations with sand content (Pearson's R = 0.510).

Table 3. PCC analysis.

	$CaCO_3$	OM	Sand	Mud	HI	^{238}U	^{232}Th	^{40}K
$CaCO_3$	1	0.488	−0.969	−0.052	−0.544	0.101	−0.123	−0.425
OM		1	−0.597	0.437	−0.172	0.357	−0.073	−0.278
Sand			1	−0.198	0.477	−0.268	0.069	0.510
Mud				1	0.227	0.678	0.217	−0.381
HI					1	0.154	0.696	−0.114
^{238}U						1	0.419	−0.312
^{232}Th							1	−0.186
^{40}K								1
	Weak		Moderate		Strong		Very Strong	

The observed HCA results (Figure 6) were remarkably similar to the PCC results. It revealed that there are two groups of variables. Cluster (1) is related to ^{40}K and sand. This suggests that ^{40}K is more linked with sand in the considered marine sediments. Cluster (2) splits into two subclusters: A (^{238}U, ^{232}Th, HI, and Mud) and B ($CaCO_3$). This indicates that ^{238}U and ^{232}Th are more associated with HI and, to a lesser extent, mud content. In addition, no possible association is noted between $CaCO_3$ and the measured radionuclides.

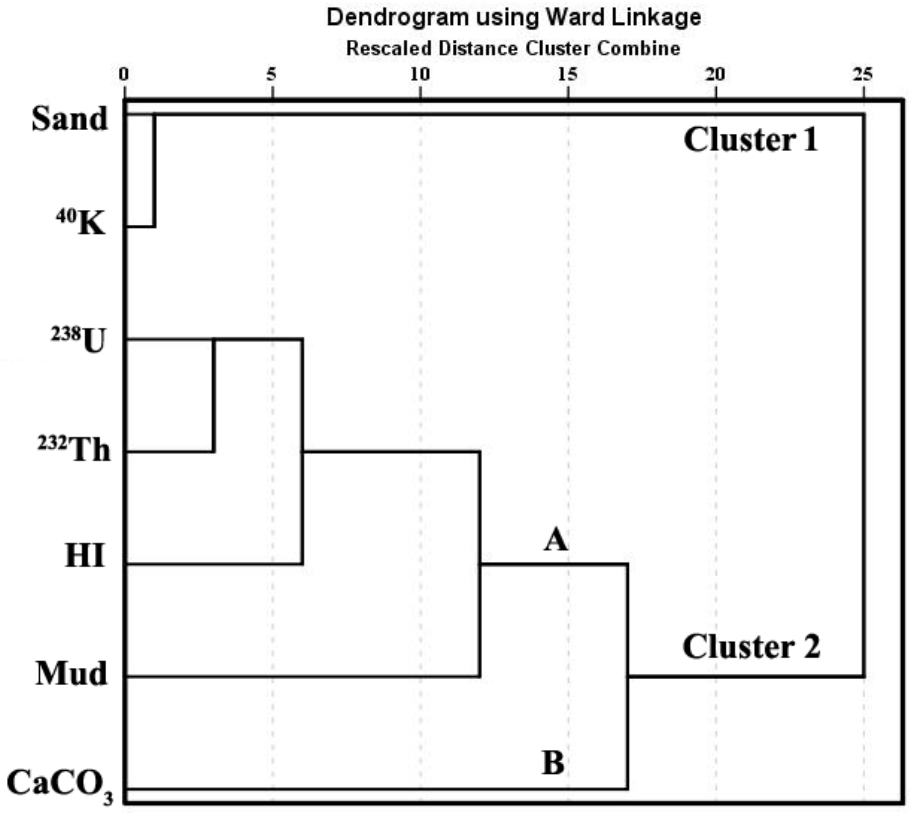

Figure 6. Q-Mode dendrogram of HCA analysis.

Figure 7 present the 3D loading of PCA component; three components (PC1 (38.92), PC2 (30.04%), and PC3 (12.47%)) were extracted. The 3D plots of the extracted three components positively confirms the findings of PCC and HCA analyses.

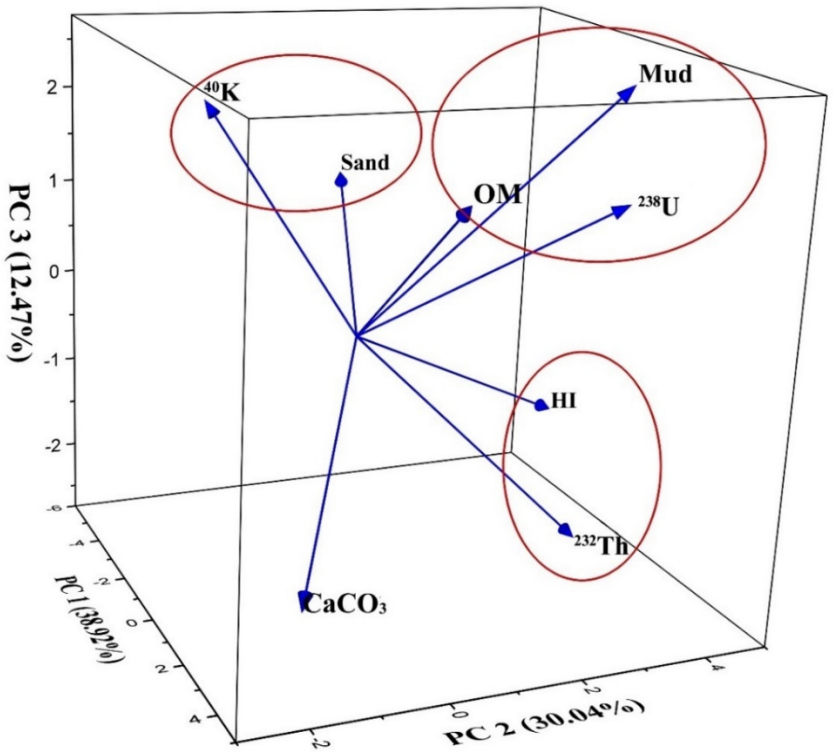

Figure 7. PCA variable 3D loading.

3.5. Radiation Hazard

3.5.1. Radiation Hazard for Humans

The calculated values of the radiological hazard parameters for the investigated marine sediments are shown in Table 4. In order to establish homogeneity with regard to radiation dose from the measured naturally occurring radionuclides, the radium equivalent activity index (Ra_{eq}) was calculated [1,59]. The obtained Ra_{eq} values ranged from 43.526 to 87.620 Bq kg^{-1} (mean 63.969 Bq kg^{-1}). These levels are considerably below 370 Bq kg^{-1}, which is the suggested maximum value [1,59]. Gamma radiation from emitting natural radionuclides in the studied marine sediment has an external hazard index (H_{ex}) that ranges from 0.118 to 0.237 (mean 0.173). All calculated H_{ex} values in this investigation are below the safety level of one [60], which is regarded as negligible. Absorbed dose rate (D) is the exposure of an individual to external, terrestrial radiation while engaged in outdoor activity. The calculated D values varied from 21.196 to 42.137 nGy h^{-1} (mean 31.493 nGy h^{-1}). These values were below the world average (57 nGy h^{-1}) [1] in all studied marine sediment samples. Figure 8 shows the contributions of ^{238}U, ^{232}Th, and ^{40}K to the obtained D values contained in each sediment sampling site. Evidently, the contribution of ^{40}K is the greater one, and the contribution of the measured radionuclides in D values varies from one site to another.

Table 4. Calculated radiological parameters in Jeddah Coast sediment.

Sample No.	Ra_{eq}	H_{ex}	D	AEDE	ELCR × 10^{-3}
1	87.620	0.237	42.137	0.052	0.181
2	48.176	0.130	24.397	0.030	0.105
3	69.589	0.188	34.339	0.042	0.147
4	69.639	0.188	33.670	0.041	0.145
5	60.678	0.164	30.460	0.037	0.131
6	60.335	0.163	30.282	0.037	0.130
7	84.667	0.229	40.130	0.049	0.172
8	60.132	0.162	30.081	0.037	0.129
9	58.778	0.159	29.443	0.036	0.126
10	76.434	0.206	36.885	0.045	0.158
11	56.253	0.152	27.039	0.033	0.116
12	43.526	0.118	21.196	0.026	0.091
13	60.058	0.162	28.776	0.035	0.124
14	72.869	0.197	36.389	0.045	0.156
15	46.991	0.127	23.775	0.029	0.102
16	77.830	0.210	38.792	0.048	0.167
17	58.688	0.158	29.377	0.036	0.126
18	59.182	0.160	29.702	0.036	0.127
Min	43.526	0.118	21.196	0.026	0.091
Max	87.620	0.237	42.137	0.052	0.181
Mean	63.969	0.173	31.493	0.039	0.135

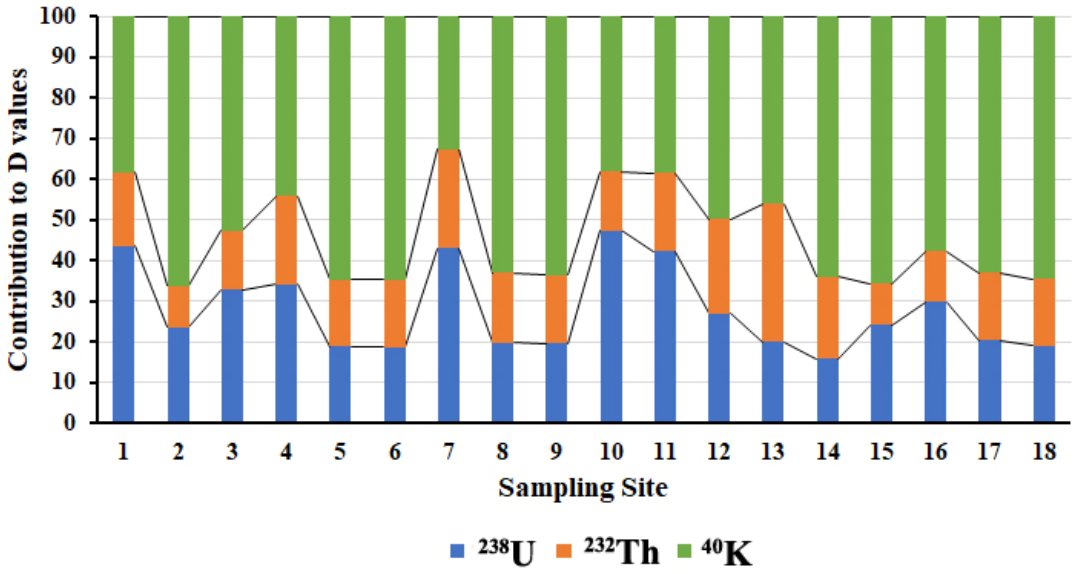

Figure 8. The contributions of ^{238}U, ^{232}Th, and ^{40}K to D values.

The annual effective doses (AEDEs) for inhabitants were calculated based on D values. AEDE values ranged from 0.026 to 0.052 mSv yr^{-1} (mean 0.039 mSv yr^{-1}). These values were lower than the worldwide average (0.07 mSv yr^{-1}) [1] in all the studied sediment samples. Long-term exposure to ionizing radiation typically leads to further risks described as excess lifetime cancer risk (ELCR). To obtain a better insight of the health effects of external exposure to the measured natural radionuclides in Jeddah coast marine sediments, ELCR factors were calculated using AEDE values. The obtained values ranged from 0.091 × 10^{-3} to 0.181 × 10^{-3} (mean 0.135 × 10^{-3}). The ELCR-calculated values are lower than the world's average (0.29 × 10^{-3}) [6,61]. This demonstrates that public exposure to the investigated marine sediments in Jeddah coastal area cannot cause cancer over the course of their lives. Figure 9 depicts the GIS-based distribution pattern maps of the calculated radiological risk parameters.

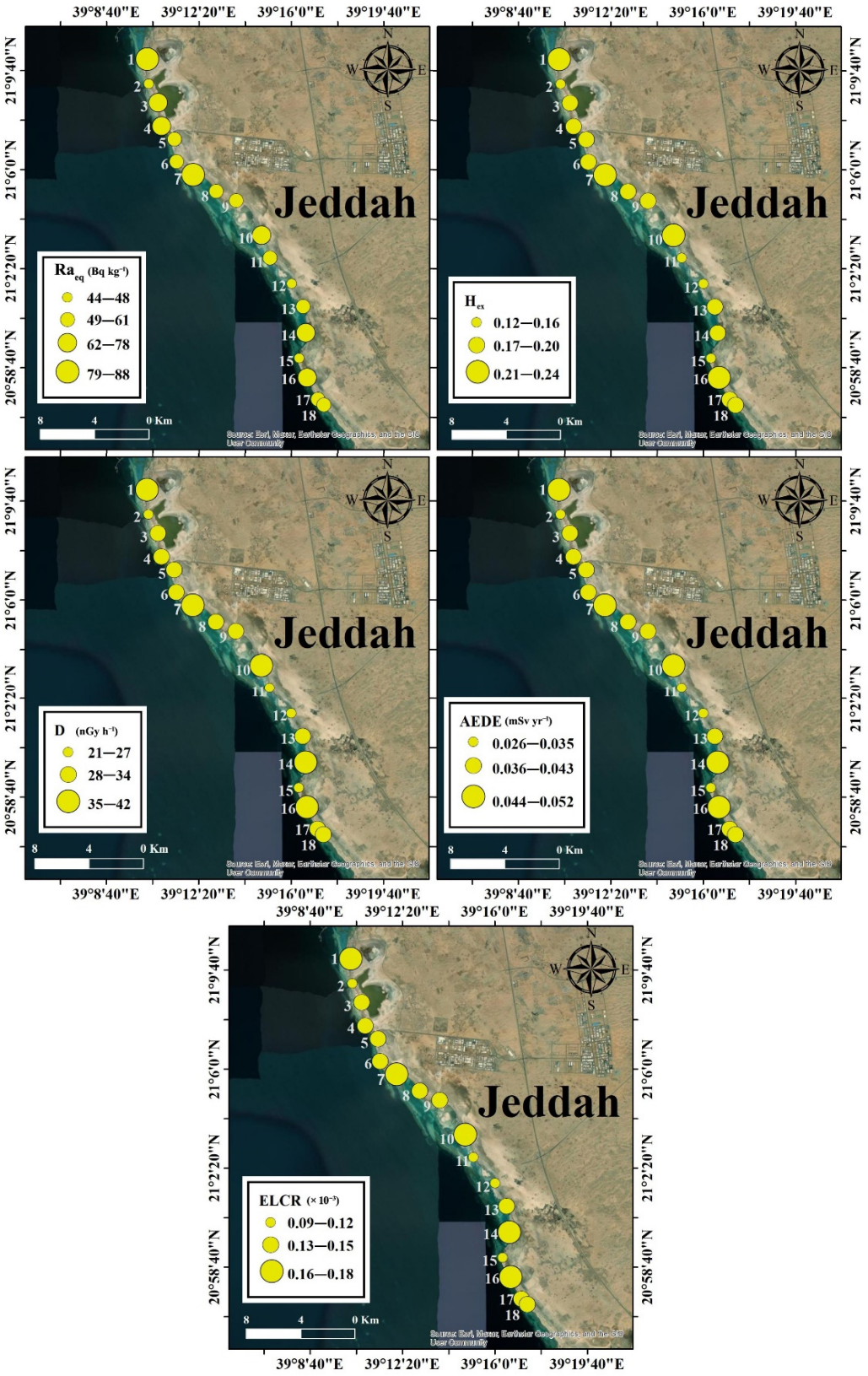

Figure 9. Distribution pattern maps of radiological risk parameters.

3.5.2. Radiation Hazard for Non-Human Biota

Using the ERICA Tool [63,64], the TD to non-human biota (marine organisms) as a result of exposure to ^{238}U and ^{232}Th in Jeddah coast marine sediments was estimated and is displayed in Table 5. As shown, the expected TD values were far below the background dose rates. The estimated TD values from Jeddah coast marine sediments radionuclide concentrations to non-human biota are not considerable biological hazards. The assessed TD values for phytoplankton and polychaete worms were considerably greater than other organisms. This indicates that sediment radioactivity may end up causing phytoplankton and polychaete worms to receive the highest dose rates. As the base of the food chain, phytoplankton can be regarded as a significant bioindicator for continuous monitoring of radiological hazard in aquatic ecosystems [31].

Table 5. Estimated TD for marine organism in Jeddah Coastline marine sediment.

Sample No.	Benthic Fish	Crustacean	Macroalgae	Mollusca–Bivalve	Pelagic Fish	Phytoplankton	Polychaete Worm	Zooplankton
1	2.84×10^{-3}	3.14×10^{-3}	2.85×10^{-2}	1.45×10^{-2}	1.72×10^{-3}	1.08×10^{-1}	3.70×10^{-1}	1.23×10^{-3}
2	8.90×10^{-4}	9.90×10^{-4}	8.92×10^{-3}	4.55×10^{-3}	5.40×10^{-4}	3.43×10^{-2}	1.16×10^{-1}	3.90×10^{-4}
3	1.75×10^{-3}	1.93×10^{-3}	1.75×10^{-2}	8.91×10^{-3}	1.05×10^{-3}	6.77×10^{-2}	2.27×10^{-1}	7.60×10^{-4}
4	1.85×10^{-3}	2.04×10^{-3}	1.79×10^{-2}	9.17×10^{-3}	1.08×10^{-3}	7.73×10^{-2}	2.32×10^{-1}	8.60×10^{-4}
5	9.60×10^{-4}	1.06×10^{-3}	9.05×10^{-3}	4.64×10^{-3}	5.40×10^{-4}	4.37×10^{-2}	1.16×10^{-1}	4.80×10^{-4}
6	9.50×10^{-4}	1.04×10^{-3}	8.88×10^{-3}	4.55×10^{-3}	5.30×10^{-4}	4.33×10^{-2}	1.14×10^{-1}	4.70×10^{-4}
7	2.74×10^{-3}	3.02×10^{-3}	2.69×10^{-2}	1.37×10^{-2}	1.61×10^{-3}	1.11×10^{-1}	3.48×10^{-1}	1.25×10^{-3}
8	1.00×10^{-3}	1.10×10^{-3}	9.38×10^{-3}	4.81×10^{-3}	5.60×10^{-4}	4.52×10^{-2}	1.21×10^{-1}	5.00×10^{-4}
9	9.60×10^{-4}	1.06×10^{-3}	9.02×10^{-3}	4.62×10^{-3}	5.40×10^{-4}	4.35×10^{-2}	1.16×10^{-1}	4.80×10^{-4}
10	2.65×10^{-3}	2.93×10^{-3}	2.70×10^{-2}	1.37×10^{-2}	1.63×10^{-3}	9.60×10^{-2}	3.52×10^{-1}	1.10×10^{-3}
11	1.78×10^{-3}	1.97×10^{-3}	1.78×10^{-2}	9.06×10^{-3}	1.07×10^{-3}	6.91×10^{-2}	2.31×10^{-1}	7.80×10^{-4}
12	9.50×10^{-4}	1.05×10^{-3}	8.96×10^{-3}	4.60×10^{-3}	5.40×10^{-4}	4.32×10^{-2}	1.15×10^{-1}	4.70×10^{-4}
13	1.09×10^{-3}	1.20×10^{-3}	9.25×10^{-3}	4.79×10^{-3}	5.40×10^{-4}	6.13×10^{-2}	1.17×10^{-1}	6.50×10^{-4}
14	1.02×10^{-3}	1.13×10^{-3}	9.11×10^{-3}	4.70×10^{-3}	5.40×10^{-4}	5.24×10^{-2}	1.16×10^{-1}	5.60×10^{-4}
15	8.90×10^{-4}	9.80×10^{-4}	8.88×10^{-3}	4.53×10^{-3}	5.40×10^{-4}	3.40×10^{-2}	1.15×10^{-1}	3.90×10^{-4}
16	1.79×10^{-3}	1.97×10^{-3}	1.79×10^{-2}	9.12×10^{-3}	1.08×10^{-3}	6.84×10^{-2}	2.32×10^{-1}	7.70×10^{-4}
17	9.90×10^{-4}	1.09×10^{-3}	9.37×10^{-3}	4.80×10^{-3}	5.60×10^{-4}	4.42×10^{-2}	1.21×10^{-1}	4.90×10^{-4}
18	9.50×10^{-4}	1.04×10^{-3}	8.91×10^{-3}	4.57×10^{-3}	5.30×10^{-4}	4.28×10^{-2}	1.15×10^{-1}	4.70×10^{-4}
Min	8.90×10^{-4}	9.80×10^{-4}	8.88×10^{-3}	4.53×10^{-3}	5.30×10^{-4}	3.40×10^{-2}	1.14×10^{-1}	3.90×10^{-4}
Max	2.84×10^{-3}	3.14×10^{-3}	2.85×10^{-2}	1.45×10^{-2}	1.72×10^{-3}	1.11×10^{-1}	3.70×10^{-1}	1.25×10^{-3}
Mean	1.45×10^{-3}	1.60×10^{-3}	1.41×10^{-2}	7.19×10^{-3}	8.40×10^{-4}	6.03×10^{-2}	1.82×10^{-1}	6.70×10^{-4}
Background Dose Rates	0.58	0.59	0.87	2	0.42	0.38	1.6	0.94

4. Conclusions

From textural and mineralogical attributes, the Jeddah coastal marine sediments are a mixture of materials of marine and continental origin. These sediments are dominated by sand fraction and $CaCO_3$ with low OM content. The identified non-opaque heavy minerals are amphiboles, pyroxenes, epidote, zircon, sphene, garnet, monazite, tourmaline, and kyanite with minor amounts of andalusite, rutile, and staurolite. The measured activity concentrations have the order of ^{40}K > ^{238}U > ^{232}Th. The mean concentration values of ^{238}U, ^{232}Th, and ^{40}K are 19.50 Bq kg^{-1}, 9.38 Bq kg^{-1}, and 403.31 Bq kg^{-1}, respectively. The radionuclide distributions were influenced by sediment mud content, organic matter, and heavy minerals index. The calculated Raeq, H_{ex}, D, AEDE, and ELCR are within the safe range and lower than the global average. The estimated TD per organism was far below the background dose rates. Natural radiation from these marine sediments is normal and poses no significant radiological risk to the public or non-human biota. The natural radioactivity of the marine sediment in this Jeddah coastline must be monitored on a regular basis to avoid unnecessary radiation exposure to the residents. Additional studies on natural radioactivity in marine water and other radionuclides level such as ^{137}Cs could provide improved insights into the status of natural radioactivity in this area. This research can assist regulatory bodies and government agencies in planning for urban and industrial expansion while keeping environmental radiation in mind.

Supplementary Materials: The following supporting information can be downloaded at: https://www.mdpi.com/article/10.3390/jmse10081145/s1, Table S1 Extensive technical descriptions of OM % and $CaCO_3$%, grain size and heavy minerals determination, and the specification of SEX/EDX and XRD instruments and ERICA tool. Table S2: Summary of the external hazard radiological parameters. Figure S1. X-ray diffractograms of bulk marine sediment samples.

Author Contributions: Conceptualization, B.A.A.-M. and A.G.; methodology, B.A.A.-M. and A.G.; software, A.G.; validation, B.A.A.-M. and A.G.; formal analysis, A.G.; investigation, B.A.A.-M. and A.G.; resources, B.A.A.-M.; data curation, A.G.; writing—original draft preparation, A.G.; writing—review and editing, B.A.A.-M. and A.G.; project administration, B.A.A.-M.; funding acquisition, B.A.A.-M. All authors have read and agreed to the published version of the manuscript.

Funding: This research work was funded by Institutional Fund Projects under grant no. (IFPIP: 126-155-1442).

Institutional Review Board Statement: Not applicable.

Informed Consent Statement: Not applicable.

Data Availability Statement: Not applicable.

Acknowledgments: This research work was funded by Institutional Fund Projects under grant no. (IFPIP: 126-155-1442). Therefore, the authors gratefully acknowledge technical and financial support from the Ministry of Education and King Abdulaziz University, DSR, Jeddah, Saudi Arabia. The authors also thank Omnia El Sayed (Ain Shams University) for providing Landsat data and helping in the application of the GIS technique. Moreover, we are indebted to Moataz Khalifa (Menoufia University), Mostafa Eid, Aya Osham, and Easra S. Ahmed (Ain Shams University) for their technical assistance.

Conflicts of Interest: The authors declare no conflict of interest. The funders had no role in the design of the study; in the collection, analyses, or interpretation of data; in the writing of the manuscript; or in the decision to publish the results.

References

1. UNSCEAR. *Sources and Effects of Ionizing Radiation, Report to the General Assembly with Scientific Annexes*; United Nation: New York, NY, USA, 2000; Available online: https://www.unscear.org/unscear/en/publications/2000_1.html (accessed on 3 July 2022).
2. Akpan, A.E.; Ebong, E.D.; Ekwok, S.E.; Eyo, J.O. Assessment of radionuclide distribution and associated radiological hazards for soils and beach sediments of Akwa Ibom Coastline, southern Nigeria. *Arab. J. Geosci.* **2020**, *13*, 753. [CrossRef]
3. Gad, A.; Saleh, A.; Khalifa, M. Assessment of natural radionuclides and related occupational risk in agricultural soil, southeastern Nile Delta, Egypt. *Arab. J. Geosci.* **2019**, *12*, 188. [CrossRef]
4. Abbasi, A.; Zakaly, H.M.H.; Mirekhtiary, F. Baseline levels of natural radionuclides concentration in sediments East coastline of North Cyprus. *Mar. Pollut. Bull.* **2020**, *161*, 111793. [CrossRef] [PubMed]
5. Abed, N.S.; Monsif, M.A.; Zakaly, H.M.H.; Awad, H.A.; Hessien, M.M.; Yap, C.K. Assessing the Radiological Risks Associated with High Natural Radioactivity of Microgranitic Rocks: A Case Study in a Northeastern Desert of Egypt. *Int. J. Environ. Res. Public Health* **2022**, *19*, 473. [CrossRef] [PubMed]
6. UNSCEAR. *Sources and Effects of Ionizing Radiation, Report to the General Assembly with Scientific Annexes*; United Nation: New York, NY, USA, 2008; Available online: https://www.unscear.org/unscear/en/publications/2008_1.html (accessed on 3 July 2022).
7. Suliman, I.I.; Alsafi, K. Radiological Risk to Human and Non-Human Biota Due to Radioactivity in Coastal Sand andMarine Sediments, Gulf of Oman. *Life* **2021**, *11*, 549. [CrossRef] [PubMed]
8. Osman, R.; Dawood, Y.H.; Melegy, A.; El-Bady, M.S.; Saleh, A.; Gad, A. Distributions and Risk Assessment of the Natural Radionuclides in the Soil of Shoubra El Kheima, South Nile Delta, Egypt. *Atmosphere* **2022**, *13*, 98. [CrossRef]
9. Abbasi, A.; Algethami, M.; Bawazeer, O.; Zakaly, H.M.H. Distribution of natural and anthropogenic radionuclides and associated radiation indices in the Southwestern coastline of Caspian Sea. *Mar. Pollut. Bull.* **2022**, *178*, 113593. [CrossRef]
10. Baghdady, A.; Awad, S.; Gad, A. Assessment of metal contamination and natural radiation hazards in different soil types near iron ore mines, Bahariya Oasis, Egypt. *Arab. J. Geosci.* **2018**, *11*, 506. [CrossRef]
11. Yehia, M.; Baghdady, A.; Howari, F.M.; Awad, S.; Gad, A. Natural radioactivity and groundwater quality assessment in the northern area of the Western Desert of Egypt. *J. Hydrol.-Reg. Stud.* **2017**, *12*, 331–344. [CrossRef]
12. Adikaram, M.; Pitawala, A.; Ishiga, H.; Jayawardana, D.; Eichler, C.M. An Ecological Risk Assessment of Sediments in a Developing Environment—Batticaloa Lagoon, Sri Lanka. *J. Mar. Sci. Eng.* **2021**, *9*, 73. [CrossRef]
13. Biswas, K.P.; Hossain, S.; Deb, N.; Bhuian, A.K.M.S.I.; Gonçalves, S.C.; Hossain, S.; Hossen, M.B. Assessment of the Levels of Pollution and of Their Risks by Radioactivity and Trace Metals on Marine Edible Fish and Crustaceans at the Bay of Bengal (Chattogram, Bangladesh). *Environments* **2021**, *8*, 13. [CrossRef]

14. Farhat, H.I. Impact of Drain Effluent on Surficial Sediments in the Mediterranean Coastal Wetland: Sedimentological Characteristics and Metal Pollution Status at Lake Manzala, Egypt. *J. Ocean Univ. China* **2019**, *18*, 834–848. [CrossRef]
15. Bantan, R.A.; Khawfany, A.A.; Basaham, A.S.; Gheith, A.M. Geochemical Characterization of Al-Lith Coastal Sediments, Red Sea, Saudi Arabia. *Arab. J. Sci. Eng.* **2020**, *45*, 291–306. [CrossRef]
16. Solomon, K. Sources of radioactivity in the ocean environment: From low level waste to nuclear powered submarines. *J. Hazard. Mater.* **1988**, *18*, 255–262. [CrossRef]
17. IAEA (International Atomic Energy Agency). *Sources of Radioactivity in the Marine Environment and Their Relative Contributions to Overall Dose Assessment from Marine Radioactivity*; MARDOS: Vienna, Austria, 1995.
18. Uddin, S.; Fowler, S.W.; Behbehani, M.; Al-Ghadban, A.N.; Swarzenski, P.W.; Al-Awadhi, N. A review of radioactivity in the Gulf region. *Mar. Pollut. Bull.* **2020**, *159*, 111481. [CrossRef]
19. Lin, M.; Qiao, J.; Hou, X.; Dellwig, O.; Steier, P.; Hain, K.; Golser, R.; Zhu, L. 70-Year Anthropogenic Uranium Imprints of Nuclear Activities in Baltic Sea Sediments. *Environ. Sci. Technol.* **2021**, *55*, 8918–8927. [CrossRef] [PubMed]
20. Al-Qasmi, H.; Law, G.T.; Fifield, L.K.; Howe, J.A.; Brand, T.; Cowie, G.L.; Law, K.A.; Livens, F.R. Deposition of artificial radionuclides in sediments of Loch Etive, Scotland. *J. Environ. Radioact.* **2018**, *187*, 45–52. [CrossRef]
21. Pappa, K.F.; Tsabaris, C.; Ioannidou, A.; Patiris, L.D.; Kaberi, H. Radioactivity and metal concentrations in marine sediments associated with mining activities in Ierissos Gulf, North Aegean Sea, Greece. *Appl. Radiat. Isot.* **2016**, *116*, 22–33. [CrossRef]
22. Aközcan, S.; Külahcı, F.; Mercan, Y. A suggestion to radiological hazards characterization of 226Ra, 232Th, 40K and 137Cs: Spatial distribution modelling. *J. Hazard. Mater.* **2018**, *353*, 476–489. [CrossRef]
23. Diab, H.M.; Ramadan, A.; Monged, M.H.E.; Shahin, M. Environmental assessment of radionuclides levels and some heavy metals pollution along Gulf of Suez, Egypt. *Environ. Sci. Pollut. Res.* **2019**, *26*, 12346–12358. [CrossRef]
24. Kotilainen, A.T.; Kotilainen, M.M.; Vartti, V.P.; Hutri, K.L.; Virtasalo, J.J. Chernobyl still with us: ^{137}Caesium activity contents in seabed sediments from the Gulf of Bothnia, northern Baltic Sea. *Mar. Pollut. Bull.* **2021**, *172*, 112924. [CrossRef] [PubMed]
25. Olszewski, G.; Andersson, P.; Lindahl, P.; Eriksson, M. On the distribution and inventories of radionuclides in dated sediments around the Swedish coast. *J. Environ. Radioact.* **2018**, *186*, 142–151. [CrossRef] [PubMed]
26. Tsabaris, C.; Patiris, D.L.; Fillis-Tsirakis, E.; Kapsimalis, V.; Pilakouta, M.; Pappa, F.K.; Vlastou, R. Vertical distribution of 137Cs activity concentration in marine sediments at Amvrakikos Gulf, western of Greece. *J. Environ. Radioact.* **2015**, *144*, 1–8. [CrossRef]
27. Heldal, H.E.; Helvik, L.; Appleby, P.; Haanes, H.; Volynkin, A.; Jensen, H.; Lepland, A. Geochronology of sediment cores from the Vefsnfjord, Norway. *Mar. Pollut. Bull.* **2021**, *170*, 112683. [CrossRef] [PubMed]
28. Baltas, H.; Sirin, M.; Dalgic, G.; Cevik, U. An overview of the ecological half-life of the 137 Cs radioisotope and a determination of radioactivity levels in sediment samples after Chernobyl in the Eastern Black Sea, Turkey. *J. Mar. Syst.* **2018**, *177*, 21–27. [CrossRef]
29. Ikenoue, T.; Takehara, M.; Morooka, K.; Kurihara, E.; Takami, R.; Ishii, N.; Kudo, N.; Utsunomiya, S. Occurrence of highly radioactive microparticles in the seafloor sediment from the pacific coast 35 km northeast of the Fukushima Daiichi nuclear power plant. *Chemosphere* **2021**, *267*, 128907. [CrossRef] [PubMed]
30. Miura, H.; Ishimaru, T.; Ito, Y.; Kurihara, Y.; Otosaka, S.; Sakaguchi, A.; Misumi, K.; Tsumune, D.; Kubo, A.; Higaki, S.; et al. First isolation and analysis of caesium-bearing microparticles from marine samples in the Pacific coastal area near Fukushima Prefecture. *Sci. Rep.* **2021**, *11*, 5664. [CrossRef]
31. Botwe, B.O.; Schirone, A.; Delbono, I.; Barsanti, M.; Delfanti, R.; Kelderman, B.; Nyarko, E.; Lens, P.L.N. Radioactivity concentrations and their radiological significance in sediments of the Tema Harbour (Greater Accra, Ghana). *J. Radiat. Res. Appl. Sci.* **2017**, *10*, 63–71. [CrossRef]
32. Bhuiyan, M.A.; Siddique, M.A.; Zafar, M.; Kamal, A.M. Spatial distribution of radioisotope concentrations in the offshore water and sediment of the Bay of Bengal (Indian Ocean), Bangladesh. *Isot. Environ. Health Stud.* **2014**, *50*, 134–141. [CrossRef]
33. Tsabaris, C.; Androulakaki, E.G.; Ballas, D.; Alexakis, S.; Perivoliotis, L.; Iona, A. Radioactivity Monitoring at North Aegean Sea Integrating In-Situ Sensor in an Ocean Observing Platform. *J. Mar. Sci. Eng.* **2021**, *9*, 77. [CrossRef]
34. Caridi, F.; Paladini, G.; Venuti, V.; Crupi, V.; Procopio, S.; Belvedere, A.; D'Agostino, M.; Faggio, G.; Grillo, R.; Marguccio, S.; et al. Radioactivity, Metals Pollution and Mineralogy Assessment of a Beach Stretch from the Ionian Coast of Calabria (Southern Italy). *Int. J. Environ. Res. Public Health* **2021**, *18*, 12147. [CrossRef] [PubMed]
35. IAEA (International Atomic Energy Agency). *Nuclear Power Reactors in the World*; Arab Atomic Energy Agency (AAEA): Vienna, Austria, 2021.
36. Damoom, M.M.; Hashim, S.; Aljohani, M.S.; Saleh, M.A.; Xoubi, N. Potential areas for nuclear power plants siting in Saudi Arabia: GIS-based multi-criteria decision making analysis. *Prog. Nucl. Energy* **2019**, *110*, 110–120. [CrossRef]
37. Ramadan, R.S.; Dawood, Y.H.; Yehia, M.M.; Gad, A. Environmental and health impact of current uranium mining activities in southwestern Sinai, Egypt. *Environ. Earth Sci.* **2022**, *81*, 213. [CrossRef]
38. WNA (World Nuclear Association). *Nuclear Power in Saudi Arabia*; World Nuclear Association: London, UK, 2017; Available online: http://www.worldnuclear.org/information-library/country-profiles/countries-o-s/saudi-arabia.aspx. (accessed on 8 January 2022).
39. Ahmad, A.; Ramana, M.V. Too costly to matter: Economics of nuclear power for Saudi Arabia. *Energy* **2014**, *69*, 682–694. [CrossRef]
40. Al Osaimi, N.M.; Qoradi, M.D. Candidate site selection for nuclear power plants in Saudi Arabia using GIS. *Arab. J. Geosci.* **2020**, *13*, 1218. [CrossRef]

41. Al-Mur, B.A.; Quicksall, A.N.; Kaste, J.M. Determination of sedimentation, diffusion, and mixing rates in coastal sediments of the eastern Red Sea via natural and anthropogenic fallout radionuclides. *Mar. Pollut. Bull.* **2017**, *122*, 456–463. [CrossRef] [PubMed]
42. Gomaa, M.N.; Mulla, D.J.; Galzki, J.C.; Sheikho, K.M.; Alhazmi, N.M.; Mohamed, H.E.; Hannachi, I.; Abouwarda, A.M.; Hassan, E.A.; Carmichael, W.W. Red Sea MODIS Estimates of Chlorophyll A and Phytoplankton Biomass Risks to Saudi Arabian Coastal Desalination Plants. *J. Mar. Sci. Eng.* **2021**, *9*, 11. [CrossRef]
43. El Zokm, G.M.; Al-Mur, B.A.; Okbah, M.A. Ecological risk indices for heavy metal pollution assessment in marine sediments of Jeddah Coast in the Red Sea. *Int. J. Environ. Anal. Chem.* **2020**, 1–22. [CrossRef]
44. Ghandour, I.M.; Basaham, S.; Al-Washmi, A.; Masuda, H. Natural and anthropogenic controls on sediment composition of an arid coastal environment: Sharm Obhur, Red Sea, Saudi Arabia. *Environ. Monit. Assess.* **2014**, *186*, 1465–1484. [CrossRef]
45. Jamoussi, B.; Chakroun, R.; Al-Mur, B. Assessment of Total Petroleum Hydrocarbon Contamination of the Red Sea with Endemic Fish from Jeddah (Saudi Arabia) as Bioindicator of Aquatic Environmental Pollution. *Water* **2022**, *14*, 1706. [CrossRef]
46. Al-Zahrany, A.A.; Farouk, M.A.; Al-Yousef, A.A. Distribution of naturally occurring radioactivity and ^{137}Cs in the marine sediment of Farasan Island, Southern Red Sea, Saudi Arabia. *Radiat. Prot. Dosim.* **2012**, *152*, 135–139. [CrossRef] [PubMed]
47. Alshahri, F. Radioactivity of ^{226}Ra, ^{232}Th, ^{40}K and ^{137}Cs in beach sand and sediment near to desalination plant in eastern Saudi Arabia: Assessment of radiological impacts. *J. King Saud Univ. Sci.* **2017**, *29*, 174–181. [CrossRef]
48. Alzahrani, J.S.; Almuqrin, A.; Alghamdi, H.; Albarzan, B.; Khandaker, M.U.; Sayyed, M.I. Radiological monitoring in some coastal regions of the Saudi Arabian Gulf close to the Iranian Bushehr nuclear plant. *Mar. Pollut. Bull.* **2022**, *175*, 113146. [CrossRef]
49. Al-Trabulsy, H.; Khater, A.; Habbani, F. Radioactivity levels and radiological hazard indices at the Saudi coastline of the Gulf of Aqaba. *Radiat. Phys. Chem.* **2011**, *80*, 343–348. [CrossRef]
50. Rifaat, A.E.; Basaham, A.S.; El-Mamoney, M.H.M.; El-Sayed, A. Mineralogical and chemical composition of dry atmospheric deposition on Jeddah city eastern coast of the Red Sea. *JKAU Mar. Sci.* **2007**, *19*, 167–188. [CrossRef]
51. Khawfany, A.A.; Aref, M.A.; Taj, R.J. Human-induced changes in sedimentary facies and depositional environments, Sarum area, Red Sea coast, Saudi Arabia. *Environ. Earth Sci.* **2017**, *76*, 61. [CrossRef]
52. Gheith, A.M.; Al Washmi, H.A.; Nabhan, A.I. Mineralogy and provenance of Ash Shuqayq coastal sediments, Southern Red Sea, Kingdom of Saudi Arabia. *JKAU Mar. Sci.* **2005**, *16*, 25–44. [CrossRef]
53. Luczak, C.; Janquin, M.A.; Kupka, A. Simple standard procedure for the routine determination of organic matter in marine sediment. *Hydrobiologia* **1997**, *345*, 87–94. [CrossRef]
54. Gross, M.G. Carbon determination. In *Procedures in Sedimentary Petrology*; Carver, R.E., Ed.; Wiley-Interscience: New York, NY, USA; pp. 573–596. 1971.
55. Lewis, D.W.; McConchie, D. *Analytical Sedimentology*; Springer: Amsterdam, The Netherlands, 1994.
56. Galehouse, J.S. Point counting. In *Procedures in Sedimentary Petrology*; Carver, R.E., Ed.; Wiley-Interscience: New York, NY, USA, 1971; pp. 385–407.
57. Mange, M.A.; Maurer, H.W. *Heavy Minerals in Colour*; Chapman Hall: London, UK, 1992; Volume 147.
58. IAEA (International Atomic Energy Agency). *Intercomparison Runs Reference Manuals*; AQCS: Vienna, Austria, 1995.
59. Beretka, J.; Mathew, P.J. Natural radioactivity of Australian building materials, industrial wastes and by-products. *Health Phys.* **1985**, *48*, 87–95. [CrossRef]
60. ECRP (European Commission Radiation Protection). *Radiological Protection Principles Concerning the Natural Radioactivity of Building Materials*; European Comission: Brussels, Belgium, 1999.
61. Taskin, H.; Karavus, M.; Ay, P.; Topuzoglu, A.; Hindiroglu, S.; Karahan, G. Radionuclide concentrations in soil and lifetime cancer risk due to the gamma radioactivity in Kirklareli, Turkey. *J. Environ. Radioact.* **2009**, *100*, 49–53. [CrossRef]
62. ICRP (International Commission on Radiological Protection). Recommendations of the International Commission on Radiological Protection. In *ICRP Publication 60*; Pergamon Press Ann ICRP: Oxford, UK, 1990.
63. Brown, J.E.; Alfonso, B.; Avila, R.; Beresford, N.A.; Copplestone, D.; Pröhl, G.; Ulanovsky, A. The ERICA tool. *J. Environ. Radioact.* **2008**, *99*, 1371–1383. [CrossRef]
64. Larsson, C.M. An overview of the ERICA Integrated Approach to the assessment and management of environmental risks from ionising contaminants. Journal of Environmental Radioactivity. *J. Environ. Radioact.* **2008**, *99*, 1364–1370. [CrossRef] [PubMed]
65. Basaham, A.S. Mineralogical and chemical composition of the mud fraction from the surface sediments of Sharm Al-Kharrar, a Red Sea coastal lagoon. *Oceanologia* **2008**, *50*, 557–575.
66. El Sabrouti, M.A. Texture and mineralogy of the surface sediments of Sharm Obhur, west Red Sea coast of Saudi Arabia. *Mar. Geol.* **1983**, *53*, 103–116. [CrossRef]
67. Basaham, A.S.; El-Shater, A. Textural and Mineralogical Characteristics of the Surficial Sediments of Sharm Obhur, Red Sea Coast of Saudi Arabia. *JKAU Mar. Sci.* **1994**, *5*, 51–57l. [CrossRef]
68. Dawood, Y.H.; Abd El-Naby, H.H. Mineral chemistry of monazite from the black sand deposits, northern Sinai, Egypt: A provenance perspective. *Miner. Mag.* **2007**, *71*, 389–406. [CrossRef]
69. Awad, M.; El Mezayen, A.M.; El Azab, A.; Alfi, S.M.; Ali, H.H.; Hanfi, M.Y. Radioactive risk assessment of beach sand along the coastline of Mediterranean Sea at El-Arish area, North Sinai, Egypt. *Mar. Pollut. Bull.* **2022**, *177*, 113494. [CrossRef]
70. Papadopoulos, A.; Koroneos, A.; Christofides, G.; Papadopoulou, L.; Tzifas, I.; Stoulos, S. Assessment of gamma radiation exposure of beach sands in highly touristic areas associated with plutonic rocks of the Atticocycladic zone (Greece). *J. Environ. Radioact.* **2016**, *162*, 235–243. [CrossRef]

71. Shuaibu, H.K.; Khandaker, M.U.; Alrefae, T.; Bradley, D.A. Assessment of natural radioactivity and gamma-ray dose in monazite rich black Sand Beach of Penang Island, Malaysia. *Mar. Pollut. Bull.* **2017**, *119*, 423–428. [CrossRef]
72. Bharath, K.M.; Natesan, U.; Chandrasekaran, S.; Srinivasalu, S. Determination of natural radionuclides and radioactive minerals in urban coastal zone of South India using Geospatial approach. *J. Radioanal. Nucl. Chem.* **2022**, *331*, 2005–2018. [CrossRef]
73. Milner, H.B.; Ward, A.M.; Highan, F. *Sedimentary Petrography, Principle and Application*, 4th ed.; The Macmillan: New York, NY, USA, 1962; Volume 11.
74. Sagga, A.M.S. The use of the textural parameters of sand in studying the characteristics and depositional processes of coastal sediments on Saudi Arabian beaches. *Mar. Geol.* **1992**, *104*, 179–186. [CrossRef]
75. Papadopoulos, A.; Christofides, G.; Koroneos, A.; Papastefanou, C.; Stoulos, S. Distribution of ^{238}U, ^{232}Th and ^{40}K in plutonic rocks of Greece. *Chem. Erde Geochem.* **2014**, *74*, 749–764. [CrossRef]
76. Drzymała, T.; Łukaszek-Chmielewska, A.; Lewicka, S.; Stec, J.; Piotrowska, B.; Isajenko, K.; Lipiński, P. Assessment of the Natural Radioactivity of Polish and Foreign Granites Used for Road and Lapidary Constructions in Poland. *Materials* **2020**, *13*, 2824. [CrossRef] [PubMed]
77. Ekpe, E.E.; Ben, U.C.; Ekwok, S.E.; Ebong, E.D.; Akpan, A.E.; Eldosouky, A.M.; Abdelrahman, K.; Gómez-Ortiz, D. Assessment of Natural Radionuclide Distribution Pattern and Radiological Risk from Rocks in Precambrian Oban Massif, Southeastern Nigeria. *Minerals* **2022**, *12*, 312. [CrossRef]
78. Caridi, F.; Messina, M.; Faggio, G.; Santangelo, S.; Messina, G.; Belmusto, G. Radioactivity, radiological risk and metal pollution assessment in marine sediments from Calabrian selected areas, southern Italy. *Eur. Phys. J. Plus* **2018**, *133*, 65. [CrossRef]
79. Khandaker, M.U.; Asaduzzaman, K.; Sulaiman, A.F.B.; Bradley, D.A.; Isinkaye, M.O. Elevated concentrations of naturally occurring radionuclides in heavy mineral-rich beach sands of Langkawi Island, Malaysia. *Mar. Pollut. Bull.* **2018**, *127*, 654–663. [CrossRef]
80. Korkulu, Z.; Özkan, N. Determination of natural radioactivity levels of beach sand samples in the black sea coast of Kocaeli (Turkey). *Radiat. Phys. Chem.* **2013**, *88*, 27–31. [CrossRef]
81. Al Shaaibi, M.; Ali, J.; Duraman, N.; Tsikouras, B.; Masri, Z. Assessment of radioactivity concentration in intertidal sediments from coastal provinces in Oman and estimation of hazard and radiation indices. *Mar. Pollut. Bull.* **2021**, *168*, 112442. [CrossRef]
82. Radomirović, M.; Stanković, S.; Mandić, M.; Jović, M.; Mandić, L.J.; Dragović, S.; Onjia, A. Spatial distribution, radiological risk assessment and positive matrix factorization of gamma-emitting radionuclides in the sediment of the Boka Kotorska Bay. *Mar. Pollut. Bull.* **2021**, *169*, 112491. [CrossRef]
83. Papadopoulos, A. ^{226}Ra/^{238}U and ^{228}Th/^{228}Ra disequilibrium as weathering indices in beach sand sediments associated with granitoids from Cyclades. Greece. *Appl. Geochem.* **2019**, *100*, 223–233. [CrossRef]
84. Zakaly, H.M.H.; Uosif, M.A.M.; Issa, S.A.M.; Tekin, H.O.; Madkour, H.; Tammam, M.; El-Taher, A.; Alharshan, G.A.; Mostafa, M.Y.A. An extended assessment of natural radioactivity in the sediments of the mid-region of the Egyptian Red Sea coast. *Mar. Pollut. Bull.* **2021**, *171*, 112658. [CrossRef] [PubMed]
85. Lin, W.; Feng, Y.; Yu, K.; Lan, W.; Wang, Y.; Mo, Z.; Ning, Q.; Feng, L.; He, X.; Huang, Y. Long-lived radionuclides in marine sediments from the Beibu Gulf, South China Sea: Spatial distribution, controlling factors, and proxy for transport pathway. *Mar. Geol.* **2020**, *424*, 106157. [CrossRef]
86. Thangam, V.; Rajalakshmi, A.; Chandrasekaran, A.; Arun, A.; Viswanathan, S.; Venkatraman, B.; Bera, S. Determination of natural radioactivity in beach sands collected along the coastal area of Tamilnadu, India using gamma ray spectrometry. *J. Radioanal. Nucl. Chem.* **2022**, *331*, 1207–1223. [CrossRef]
87. Evans, J.D. *Straight Forward Statistics for the Behavioral Sciences*; Brook/Cole Publishing: Pacific Grove, CA, USA, 1996.
88. Papadopoulos, A.; Koroneos, A.; Christofides, G.; Stoulos, S. Natural radioactivity distribution and gamma radiation exposure of beach sands close to Kavala pluton, Greece. *Open Geosci.* **2015**, *1*, 407–422. [CrossRef]